

How interacting Bose gases scatter light

Konstantinos Konstantinou,¹ Yansheng Zhang,¹ Paul H. C. Wong,¹ Feiyang Wang,¹ Yu-Kun Lu,² Nishant Dogra,¹ Christoph Eigen,¹ Tanish Satoor,¹ Wolfgang Ketterle,² and Zoran Hadzibabic¹

¹*Cavendish Laboratory, University of Cambridge, J. J. Thomson Avenue, Cambridge CB3 0HE, United Kingdom*

²*Research Laboratory of Electronics, MIT-Harvard Center for Ultracold Atoms,*

Department of Physics, Massachusetts Institute of Technology, Cambridge, 02139 Massachusetts, USA

The innate tendency of identical bosons to bunch, seen in the Hanbury Brown–Twiss effect [1] and Bose–Einstein condensation [2, 3], is a primary manifestation of quantum statistics. This tendency can enhance the rates of fundamental processes such as atom-atom [4] and atom-light scattering [5] if the atoms scatter into already occupied quantum states. For non-interacting bosons, the enhancement of light scattering is simply given by the bosonic-stimulation factor $1 + N_f$, where N_f is the occupation of the atom’s final momentum state. Here, we study scattering between off-resonant light and atoms in a quasi-homogeneous Bose gas with tunable interactions and show that even weak interactions, which do not significantly alter the momentum distribution, have a dramatic effect on the atom-light scattering. Due to (spatially local) beyond-mean-field atomic correlations, weak repulsive interactions can completely suppress the bosonic enhancement of scattering, while attractive ones increase the scattering rate. Moreover, if the interactions are rapidly tuned, light scattering reveals correlation dynamics that are orders of magnitude faster than the momentum-space population dynamics. Its extreme sensitivity to dynamical beyond-mean-field effects makes off-resonant light scattering a simple and powerful probe of many-body physics in ultracold atomic gases.

Scattering experiments have played a pivotal role in condensed matter physics, from the discoveries of crystal [6–8] and quasi-crystal [9] structures to the studies of critical phenomena [10] and superfluidity [11]. In a typical experiment, the particles in the probe beam, such as photons, electrons, or neutrons, interact only weakly with the system under investigation, and the correlations in the system are revealed because the interference of different scattering events affects the observed scattering rate.

Recently, such experiments were used to observe quantum-statistical correlations in ultracold atomic gases [5, 12–14]. If a high-temperature ideal gas is illuminated by an off-resonant laser, the intensity of the scattered light is simply proportional to the number of illuminated atoms. However, at high-phase space density (in quantum-degenerate gases), the innate tendency of identical bosons to bunch and fermions to anti-bunch leads to an enhancement (bosonic stimulation) of scattering for bosons and a suppression (Pauli blocking) for fermions. These effects were predicted more than 30 years ago [15–20], but observed only recently, in harmonically trapped Bose [5] and Fermi [12–14] gases.

Here, we study scattering between off-resonant light and atoms in a quasi-homogeneous Bose gas, and show that, due to beyond-mean-field (BMF) correlations, even weak and short-ranged atomic interactions can dramatically suppress or further increase the bosonically enhanced scattering rate. This interplay of bosonic statistics and atomic interactions is not captured by the standard picture of bosonic stimulation, and makes light scattering a powerful probe of both equilibrium and non-equilibrium many-body physics in quantum gases.

Our experiments are based on a ³⁹K gas held in an optical box trap [21, 22], close to the critical temperature for Bose–Einstein condensation, T_c , and with tunable contact interactions characterized by the s -wave scattering length a . Our trap is formed by intersecting two hollow-tube blue-detuned laser

beams with diameters of 35 μm and 100 μm (see Fig. 1a and Methods), and we start by preparing $N = (4 - 12) \times 10^5$ atoms in the $|F, m_F\rangle = |1, -1\rangle$ hyperfine ground state. The gas density, $n = (5 - 15) \mu\text{m}^{-3}$, is almost uniform across the cloud, and $T_c = (140 - 270) \text{ nK}$. The interactions in our clouds are always weak in the sense that $|a|$ is much smaller than both the typical inter-particle spacing $d = n^{-1/3}$ and the thermal de Broglie wavelength $\lambda = \sqrt{2\pi\hbar^2/(mk_B T)}$, and they do not significantly affect T_c or the gas density distribution (here \hbar is the reduced Planck constant, m the atom mass, and k_B the Boltzmann constant).

We illuminate the gas with an off-resonant laser beam (detuned by 1 GHz from the D2 line at 766.7 nm), and detect photons scattered at an angle of 35° (Fig. 1a). The laser intensity and pulse duration are chosen such that the cloud is only weakly perturbed (Extended Data Fig. 1), so we probe correlations that are native to the gas and avoid light-induced effects such as super-radiance [23, 24]. In this case, the scattering rate Γ at recoil momentum $\hbar\mathbf{Q}$ is given by [25–27]

$$\frac{\Gamma}{\Gamma_0} = 1 + \frac{1}{N} \iint d^3\mathbf{r}_1 d^3\mathbf{r}_2 e^{i\mathbf{Q}\cdot(\mathbf{r}_1-\mathbf{r}_2)} \times \text{Tr}[\rho \hat{\psi}^\dagger(\mathbf{r}_1)\hat{\psi}^\dagger(\mathbf{r}_2)\hat{\psi}(\mathbf{r}_2)\hat{\psi}(\mathbf{r}_1)], \quad (1)$$

where Γ_0 is the single-particle scattering rate, $\hat{\psi}(\mathbf{r})$ the bosonic field operator, and ρ the system’s thermal density matrix. Note that here the enhancement factor $E = \Gamma/\Gamma_0$ is simply the structure factor $S(\mathbf{Q})$.

As we sketch in Fig. 1b, in an ideal ($a = 0$) gas close to T_c , where $\lambda \approx d$, the scattering rate is enhanced as the overlap of the atomic wave-packets and the bosonic symmetry of the wavefunction lead to enhanced density fluctuations. In this simple $a = 0$ case, and for a uniform gas, the second-order

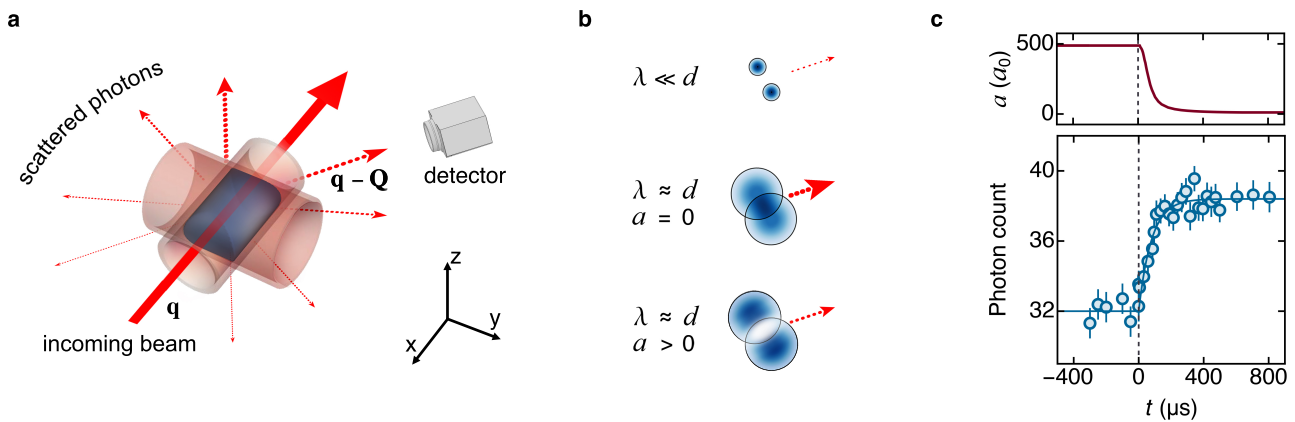


FIG. 1. **Bosonic enhancement of atom-light scattering in an interacting gas.** **a**, Experimental concept. We illuminate a quasi-homogeneous Bose gas (blue) held in an optical box trap (red) with an off-resonant laser beam and detect photons scattered at an angle of 35° . Scattering of photons from wavevector \mathbf{q} to $\mathbf{q} - \mathbf{Q}$ corresponds to atom recoil $\hbar\mathbf{Q}$. **b**, Cartoon of the effects of quantum degeneracy and atomic interactions on atom-light scattering. Here d is the inter-particle spacing (set by the gas density), λ is the thermal de Broglie wavelength (the size of the blue atomic wave-packets), and the s -wave scattering length a gives the strength of interactions. The scattered-light intensity is indicated by the thickness of the red arrows. In a degenerate non-interacting gas, with $\lambda \gtrsim d$ and $a = 0$, scattering is enhanced by interference of light scattered by overlapping wave-packets. However, this overlap and enhancement are reduced by repulsive interactions ($a > 0$). **c**, Illustration of the local beyond-mean-field effect of interactions; here $T \approx 1.1 T_c$, where $T_c \approx 200$ nK is the critical temperature for Bose–Einstein condensation. Reducing a from $500 a_0$ to $< 50 a_0$ within $200 \mu\text{s}$ (top panel) enhances atom-light scattering on the same timescale (bottom panel), which is too short to change the global momentum-space occupations or the gas density distribution (see text). For each measurement, at different times during the interaction ramp, the light pulse was applied for $10 \mu\text{s}$, and the single-particle scattering rate Γ_0 corresponds to 27 photon counts. Here, and throughout the paper, each data point is an average of at least 50 measurements, and the error bars show standard measurement errors.

correlator in Eq. (1) factorizes into first-order correlators, and

$$E = \frac{\Gamma}{\Gamma_0} = \frac{1}{N} \sum_{\mathbf{k}} N_{\mathbf{k}}(1 + N_{\mathbf{k}+\mathbf{Q}}), \quad (2)$$

where $N_{\mathbf{k}}$ is the occupation of the momentum state \mathbf{k} . This is the standard, more familiar bosonic-stimulation result. In the textbook picture, the rate of a physical process is enhanced by a factor of $1 + N_f$, where N_f is the number of bosons already occupying the final quantum state, and here the relevant states are the final momentum states, $\mathbf{k} + \mathbf{Q}$, of the recoiling atoms. The same picture is also commonly used to explain a bosonically enhanced rate of elastic atom-atom scattering, for example during formation of a Bose-Einstein condensate [4].

However, as we also sketch in Fig. 1b (bottom cartoon), repulsive interactions ($a > 0$) suppress the wave-packet overlap and the resulting enhancement [5, 28]. In this case Eq. (1) does not reduce to Eq. (2), and the scattering rate cannot be understood in terms of momentum-space occupations. Physically, the key point is that the momentum states are spatially delocalized, while bosonic enhancement fundamentally arises from spatially local correlations, through the interference of light scattered by two nearby atoms, and only for non-interacting particles the pictures in terms of local correlations and global state occupations are (mathematically) equivalent.

Indeed, in our experiments the interactions dramatically affect light scattering without significantly changing the momentum-space occupations; in fact, they affect it on a timescale on which $N_{\mathbf{k}}$ cannot change. We illustrate this in Fig. 1c, by showing how Γ grows when the interactions are

rapidly turned off. Here $T \approx 1.1 T_c$ and Γ_0 corresponds to 27(3) photon counts (Methods). Using a magnetic Feshbach resonance at 33.6 G, we first prepare the cloud at a relatively large $a = 500 a_0$, where a_0 is the Bohr radius. We then sweep the B field to reduce a to $< 50 a_0$ within $200 \mu\text{s}$ (top panel), and observe that Γ grows on the same timescale (bottom panel). For comparison, it takes several milliseconds for the global momentum-space occupations and density distribution to change [the rates of these processes are set, respectively, by the collision rate, $8\pi n a^2 \sqrt{2k_B T}/(\pi m)$, and the speed of first sound, $\approx \sqrt{k_B T/m}$]. This separation of timescales clearly shows that the change in Γ arises due to local BMF correlations.

We now turn to a quantitative study of the bosonic enhancement factor E for a range of temperatures, gas densities, and interaction strengths (Fig. 2).

Starting with the case of a quasi-ideal gas ($a = 25 a_0$, corresponding to $a/\lambda < 3 \times 10^{-3}$), in Fig. 2a we plot E as a function of T/T_c for three different densities. Near T_c , in our densest clouds we observe enhancement up to a factor of 2.

We reproduce these observations in numerical calculations (solid lines in Fig. 2a) based on Eq. (2), without considering any BMF correlations. Our simulations take into account that: (i) the gas density depends slightly on the temperature and mean-field interaction energy because the trap walls are not infinitely steep (see Methods and Extended Data Fig. 2), and (ii) Eqs. (1, 2) assume spin-preserving scattering, but in our experiments about a quarter of the scattering events are spin-changing (see Methods and Extended Data Fig. 3), and this

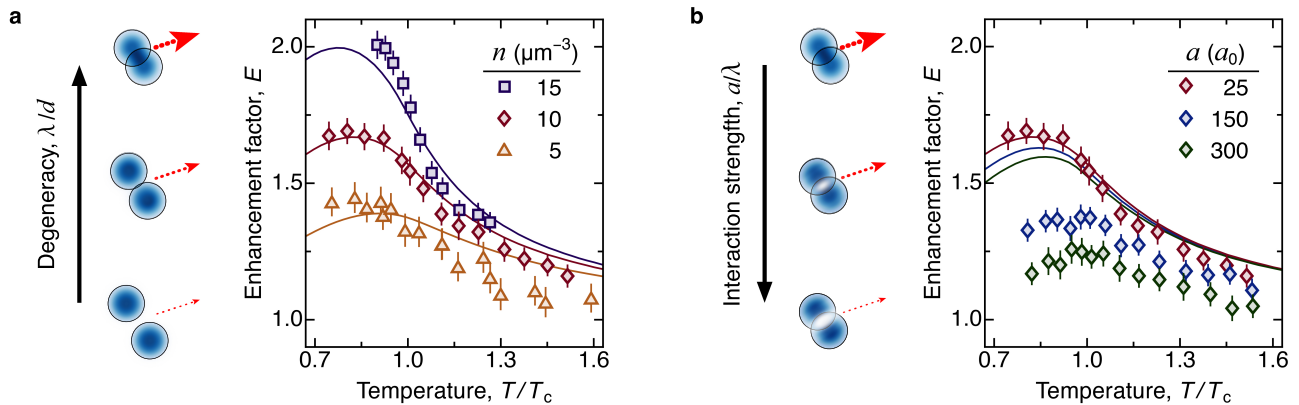


FIG. 2. **Effects of quantum degeneracy and interactions.** **a**, The bosonic enhancement factor, $E = \Gamma/\Gamma_0$, as a function of the reduced temperature T/T_c for a quasi-ideal gas ($a = 25 a_0$). The increase of enhancement with the gas density n or when approaching condensation is captured well by mean-field numerical calculations (solid lines). **b**, E versus T/T_c for different interaction strengths and fixed $n = 10 \mu\text{m}^{-3}$. Mean-field interaction effects (the differences between the three solid lines) do not explain the dramatic suppression of bosonic enhancement.

Raman process is not bosonically enhanced [5].

However, as we show in Fig. 2b, for stronger interactions (at fixed density), bosonic enhancement is dramatically suppressed over our whole temperature range, and only a small fraction of this suppression is explained by the mean-field calculations (solid lines) based on Eq. (2).

We now focus on the BMF effects on E , including their dynamics, for fixed $n = 10 \mu\text{m}^{-3}$ and $T = T_c$ (Fig. 3). Here we employ two atomic spin states, $|1, -1\rangle$ and $|1, 0\rangle$, which due to different Feshbach resonances have different values of a at the same B field (see Fig. 3a), and use two-photon (Raman) spin flips to realize sub- μs interaction quenches (see Methods and Extended Data Fig. 4). This allows us to probe purely BMF effects of changes in a , on timescales on which the global density and momentum distributions do not change.

In Fig. 3b, we show $E(t)$ for spin flips at three different B fields. In one measurement (blue), a is the same before and after the flip, and we verify that E remains the same. When we suddenly decrease or increase a (red and green, respectively), the value of E adjusts in $\approx 50 \mu\text{s}$, independently of the quench direction; the exponential fits shown by the solid lines give a time constant $\tau = 25(5) \mu\text{s}$. Since τ is much longer than the sub- μs spin flip, and much shorter than the millisecond mean-field timescales, it reflects the intrinsic timescale for the growth or decay of the BMF correlations; note that, in contrast, in Fig. 1c the rate at which Γ changes is limited by how fast a changes.

In Fig. 3c we summarize our results for interaction quenches at a range of fields (shaded regions in Fig. 3a) where a in the initial $|1, -1\rangle$ state is always small, $(25 - 40) a_0$, while a in the final $|1, 0\rangle$ state varies between $35 a_0$ and $750 a_0$. We measure E at $t = 50 \mu\text{s}$ after the spin flip, when the BMF correlations have (essentially) fully adjusted. Plotting E versus the dimensionless interaction strength a/λ shows that a scattering length that is an order of magnitude smaller than the size of the atomic wave packets (and the typical inter-particle separation) is sufficient to almost completely suppress the bosonic enhancement

of light scattering.

This suppression is captured well by considering correlation effects at the two-body level [5, 28], which effectively amounts to replacing

$$N_f \rightarrow N_f \left(1 - c \frac{a}{\lambda}\right) \quad (3)$$

in the standard $1 + N_f$ expression for the bosonically enhanced scattering events; here c is a momentum-independent factor (see Methods and Extended Data Figs. 5 and 6). In the high-temperature limit $c = 8\sqrt{2}$, and for our experiments at T_c we numerically obtain a similar value $c \approx 12$. The fact that $c \gg 1$ reflects the extreme sensitivity of light scattering to BMF effects. In Fig. 3c the solid line shows our calculated steady-state E , and the dashed line takes into account the fact that in 2τ the correlations do not yet fully settle.

Our dynamical simulations also reproduce the characteristic timescale of $25 \mu\text{s}$ for the change in correlations after quenches from either a small to large a or vice versa (see Methods and Extended Data Fig. 7). Our calculations give that well above T_c the time for the relaxation of correlations scales as $m\lambda/(\hbar Q)$; this can be understood as thermal dephasing, with the relaxation time corresponding to the time it takes particles with typical thermal velocity $\hbar/(m\lambda)$ to travel the distance $1/Q$, over which the correlations are probed. However, for $T \rightarrow T_c$ the relaxation time grows (Methods), suggesting sensitivity of light scattering to critical behavior.

Finally, in Fig. 4 we briefly explore the effect of attractive interactions ($a < 0$), still for $n = 10 \mu\text{m}^{-3}$ and $T = T_c$, and still starting in the $|1, -1\rangle$ state. Here we use spin flips to $|1, 0\rangle$ near the 65.7 G resonance to rapidly quench a from $\approx 30 a_0$ to $\pm 250 a_0$. We observe that attractive interactions increase the scattering rate above the ideal-gas level ($E \approx 1.5$, see also Fig. 3c). Moreover, at post-quench times of order τ , the effects of quenching to $\pm 250 a_0$ are essentially symmetric, as theoretically expected at leading order in a/λ ; at longer times the $a < 0$ dynamics are more complicated and

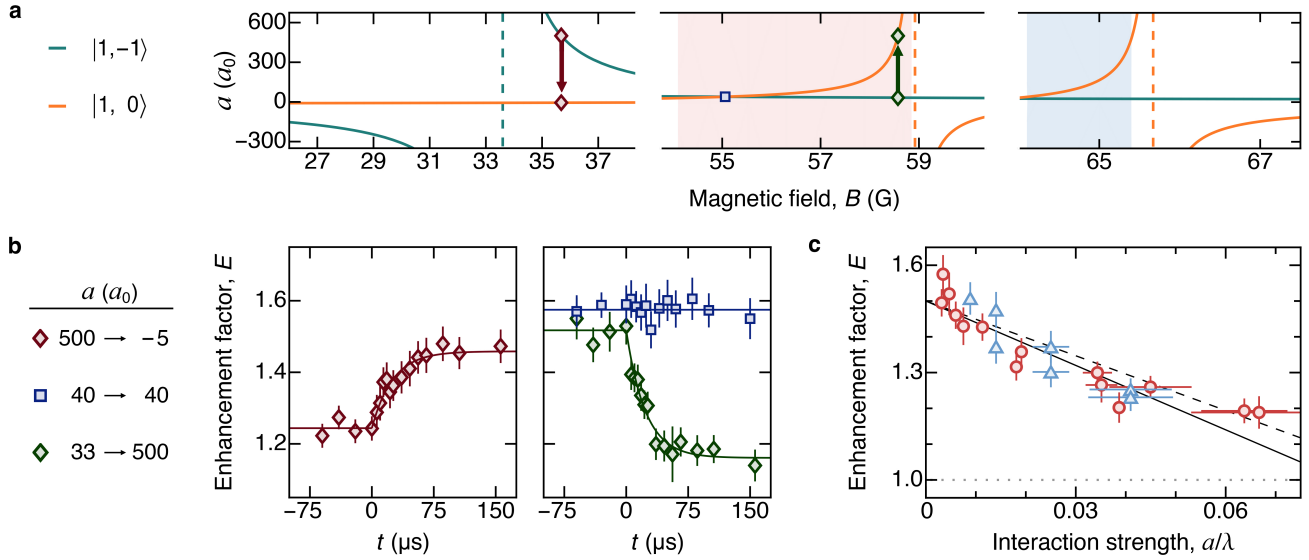


FIG. 3. **Beyond-mean-field (BMF) interaction effects.** Here we fix $n = 10 \mu\text{m}^{-3}$ and $T = T_c$, and perform spin-flips from the $|1, -1\rangle$ to the $|1, 0\rangle$ atomic state at different magnetic fields to realize sub- μs interaction quenches and study the subsequent evolution of E on microsecond timescales, when only the BMF effects can change. For all data, E is measured using $4 \mu\text{s}$ -long light-scattering pulses. **a**, $a(B)$ for the two spin states, with the dashed lines indicating Feshbach resonances (where $|a| \rightarrow \infty$). The symbols and arrows depict the spin-flips in **b**, and the shaded regions show the B -field ranges, near two different $|1, 0\rangle$ resonances, used in **c**. **b**, BMF dynamics. Independently of the initial and final value of a , BMF correlations adjust to the quench at $t = 0$ within the same time of $\approx 50 \mu\text{s}$; exponential fits (solid lines) give a time-constant $\tau = 25(5) \mu\text{s}$. **c**, Quasi-steady-state E , measured $50 \mu\text{s}$ after the quench from $a < 40 a_0$ in $|1, -1\rangle$ to $a = (35 - 750) a_0$ in $|1, 0\rangle$; the symbol colors match the shadings in **a**. Due to the small pre-quench a , all mean-field effects are negligible, and the observed suppression of E is a purely BMF effect. Plotting E versus a/λ shows that a scattering length an order of magnitude smaller than the size of the wave packets and the inter-particle distance (see Fig. 1b) is sufficient to almost completely suppress bosonic enhancement. The solid line shows the steady-state E predicted by our BMF theory (see text) and the dashed line includes the correction for the fact that in 2τ the correlations do not yet fully settle.

we do not presently understand them. Note that we do not explore stronger attractive interactions because, for the same $|a|$, particle loss due to three-body recombination is generally more severe for $a < 0$ [29, 30]; this loss is negligible over $200 \mu\text{s}$ at $-250 a_0$, and at $750 a_0$, but at $-600 a_0$ we observe 30% atom loss within $100 \mu\text{s}$.

In summary, our work sheds new light on the fundamental phenomenon of bosonic stimulation, relevant across many fields, and establishes off-resonant light scattering as a powerful new tool for probing second-order correlations in ultracold atomic gases [31–40]. In the future, probing light scattering at different angles would allow studies of correlations on different lengthscales, which could, for example, provide new insights into the critical behavior near T_c . Moreover, our methods are also applicable to far-from-equilibrium systems, such as Bose gases quenched to unitarity (where $a > \lambda, d$) [41, 42] and turbulent gases [43, 44], which are generally less understood; so far these systems have been characterized by their statistically averaged momentum distributions (*i.e.*, first-order correlations), while second-order correlations could reveal their fluctuations, including intermittency in quasi-stationary turbulence [45, 46].

Our work also raises new conceptual questions and invites complementary experiments in other systems. The suppression and enhancement of light scattering imply a modification of the real-space bunching of bosons, which should be directly

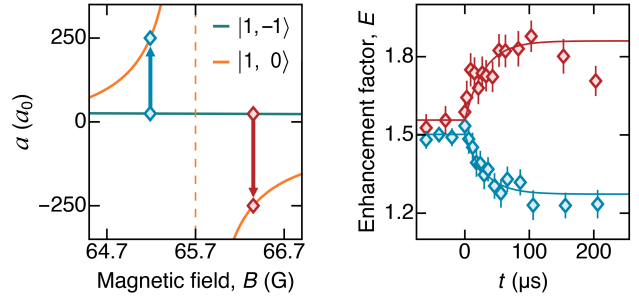


FIG. 4. **Effect of attractive interactions.** Left: Experimental protocol. We prepare the gas in a weakly interacting $|1, -1\rangle$ state and then quench at $t = 0$ to either $a = 250 a_0$ or $a = -250 a_0$ in the $|1, 0\rangle$ state. Right: Post-quench BMF dynamics. Attractive interactions increase the bosonic enhancement of atom-light scattering above the ideal-gas level ($E \approx 1.5$). At times of order $\tau \approx 25 \mu\text{s}$, the interaction effects are essentially symmetric for $a = \pm 250 a_0$, as theoretically expected to leading order in a/λ . The solid lines show exponential fits to the data for $t < 110 \mu\text{s}$ with fixed $\tau = 25 \mu\text{s}$.

observable with quantum-gas microscopes [37–40]. Interactions should also modify the bosonic enhancement of elastic atom-atom scattering, seen in the formation of a Bose–Einstein condensate [4]. Moreover, since in equilibrium the scattering into and out of the condensate are related by detailed balance,

this raises the question whether the modification of bosonic stimulation has a thermodynamic signature in the equilibrium condensed fraction. It would also be interesting to study the effects of contact interactions on the fermionic suppression of light scattering [12–14], and the effects of long-range (dipolar) interactions on both bosonic stimulation and fermionic suppression. Finally, another intriguing question is whether emission of light that is bosonically stimulated by the occupation of the final photon states (rather than the final atom states) can also be modified by some form of photon-photon [47] or emitter-photon interactions.

We thank Christopher J. Ho, Gevorg Martirosyan, Jiří Etrych, Martin Gazo, Andrey Karailiev, and Yi Jiang for discussions and comments on the manuscript. The Cambridge work was supported by EPSRC [Grant No. EP/Y01510X/1], ERC [UniFlat], and STFC [Grants No. ST/T006056/1 and No. ST/Y004469/1]. Z.H. acknowledges support from the Royal Society Wolfson Fellowship. The MIT work was supported from the NSF through grant No. PHY-2208004, from the Center for Ultracold Atoms (an NSF Physics Frontiers Center) through grant No. PHY-2317134, and the Army Research Office (contract No. W911NF2410218). Y.-K.L. is supported by the NTT Research Fellowship.

-
- [1] R. Hanbury Brown and R. Q. Twiss, Correlation between photons in two coherent beams of light, *Nature* **177**, 27 (1956).
- [2] M. H. Anderson, J. R. Ensher, M. R. Matthews, C. E. Wieman, and E. A. Cornell, Observation of Bose–Einstein condensation in a dilute atomic vapor, *Science* **269**, 198 (1995).
- [3] K. B. Davis, M. O. Mewes, M. R. Andrews, N. J. van Druten, D. S. Durfee, D. M. Kurn, and W. Ketterle, Bose–Einstein Condensation in a Gas of Sodium Atoms, *Phys. Rev. Lett.* **75**, 3969 (1995).
- [4] H.-J. Miesner, D. M. Stamper-Kurn, M. R. Andrews, D. S. Durfee, S. Inouye, and W. Ketterle, Bosonic Stimulation in the Formation of a Bose–Einstein Condensate, *Science* **279**, 1005 (1998).
- [5] Y.-K. Lu, Y. Margalit, and W. Ketterle, Bosonic stimulation of atom-light scattering in an ultracold gas, *Nat. Phys.* **19**, 210 (2023).
- [6] W. L. S. Bragg, The Structure of Some Crystals as Indicated by Their Diffraction of X-rays, *Proc. R. Soc. A* **89**, 248 (1913).
- [7] C. Davisson and L. H. Germer, Diffraction of electrons by a crystal of nickel, *Phys. Rev.* **30**, 705 (1927).
- [8] B. N. Brockhouse, Slow neutron spectroscopy and the grand atlas of the physical world, *Rev. Mod. Phys.* **67**, 735 (1995).
- [9] D. Shechtman, I. Blech, D. Gratias, and J. W. Cahn, Metallic phase with long-range orientational order and no translational symmetry, *Phys. Rev. Lett.* **53**, 1951 (1984).
- [10] N. C. Ford and G. B. Benedek, Observation of the spectrum of light scattered from a pure fluid near its critical point, *Phys. Rev. Lett.* **15**, 649 (1965).
- [11] A. D. B. Woods and R. A. Cowley, Structure and excitations of liquid helium, *Rep. Prog. Phys.* **36**, 1135 (1973).
- [12] A. B. Deb and N. Kjærgaard, Observation of Pauli blocking in light scattering from quantum degenerate fermions, *Science* **374**, 972 (2021).
- [13] Y. Margalit, Y.-K. Lu, F. Çağrı Top, and W. Ketterle, Pauli blocking of light scattering in degenerate fermions, *Science* **374**, 976 (2021).
- [14] C. Sanner, L. Sonderhouse, R. B. Hutson, L. Yan, W. R. Milner, and J. Ye, Pauli blocking of atom–light scattering, *Science* **374**, 979 (2021).
- [15] B. Svistunov and G. Shlyapnikov, Resonance optics of the low-temperature quantum gases H and D, *Sov. Phys. JETP* **70**, 460 (1990).
- [16] H. D. Politzer, Light incident on a Bose-condensed gas, *Phys. Rev. A* **43**, 6444 (1991).
- [17] J. Javanainen, Optical Signatures of a Tightly Confined Bose Condensate, *Phys. Rev. Lett.* **72**, 2375 (1994).
- [18] O. Morice, Y. Castin, and J. Dalibard, Refractive index of a dilute Bose gas, *Phys. Rev. A* **51**, 3896 (1995).
- [19] J. Javanainen and J. Ruostekoski, Off-resonance light scattering from low-temperature Bose and Fermi gases, *Phys. Rev. A* **52**, 3033 (1995).
- [20] H. D. Politzer, Bose-stimulated scattering off a cold atom trap, *Phys. Rev. A* **55**, 1140 (1997).
- [21] A. L. Gaunt, T. F. Schmidutz, I. Gotlibovych, R. P. Smith, and Z. Hadzibabic, Bose–Einstein Condensation of Atoms in a Uniform Potential, *Phys. Rev. Lett.* **110**, 200406 (2013).
- [22] N. Navon, R. P. Smith, and Z. Hadzibabic, Quantum gases in optical boxes, *Nat. Phys.* **17**, 1334 (2021).
- [23] R. H. Dicke, Coherence in spontaneous radiation processes, *Phys. Rev.* **93**, 99 (1954).
- [24] S. Inouye, A. P. Chikkatur, D. M. Stamper-Kurn, J. Stenger, D. E. Pritchard, and W. Ketterle, Superradiant Rayleigh Scattering from a Bose–Einstein Condensate, *Science* **285**, 571 (1999).
- [25] M. Lewenstein, L. You, J. Cooper, and K. Burnett, Quantum field theory of atoms interacting with photons: Foundations, *Phys. Rev. A* **50**, 2207 (1994).
- [26] J. Ruostekoski and J. Javanainen, Quantum field theory of cooperative atom response: Low light intensity, *Phys. Rev. A* **55**, 513 (1997).
- [27] J. Javanainen, J. Ruostekoski, B. Vestergaard, and M. R. Francis, One-dimensional modeling of light propagation in dense and degenerate samples, *Phys. Rev. A* **59**, 649 (1999).
- [28] M. Naraschewski and R. J. Glauber, Spatial coherence and density correlations of trapped Bose gases, *Phys. Rev. A* **59**, 4595 (1999).
- [29] T. Kraemer, M. Mark, P. Waldburger, J. G. Danzl, C. Chin, B. Engeser, A. D. Lange, K. Pilch, A. Jaakkola, H.-C. Nägerl, and R. Grimm, Evidence for Efimov quantum states in an ultracold gas of caesium atoms, *Nature* **440**, 315 (2006).
- [30] M. Zaccanti, B. Deissler, C. D’Errico, M. Fattori, M. Jonas, S. Müller, G. Roati, M. Inguscio, and G. Modugno, Observation of an Efimov spectrum in an atomic system, *Nat. Phys.* **5**, 586 (2009).
- [31] T. Jelts, J. M. McNamara, W. Hogervorst, W. Vassen, V. Krachmalnicoff, M. Schellekens, A. Perrin, H. Chang, D. Boiron, A. Aspect, and C. I. Westbrook, Comparison of the Hanbury Brown–Twiss effect for bosons and fermions, *Nature* **445**, 402 (2007).
- [32] C.-L. Hung, X. Zhang, L.-C. Ha, S.-K. Tung, N. Gemelke, and C. Chin, Extracting density–density correlations from in situ images of atomic quantum gases, *New J. Phys.* **13**, 075019 (2011).
- [33] A. Perrin, R. Bücke, S. Manz, T. Betz, C. Koller, T. Plisson, T. Schumm, and J. Schmiedmayer, Hanbury Brown and Twiss correlations across the Bose–Einstein condensation threshold, *Nat. Phys.* **8**, 195 (2012).
- [34] C.-L. Hung, V. Gurarie, and C. Chin, From Cosmology to Cold

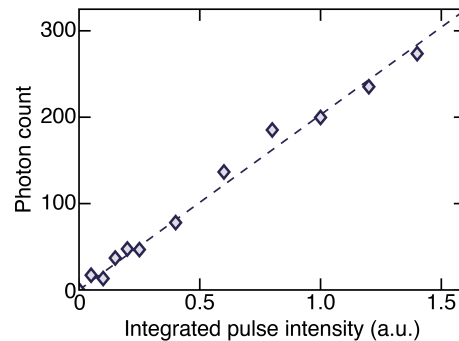
Atoms: Observation of Sakharov Oscillations in a Quenched Atomic Superfluid, *Science* **341**, 1213 (2013).

- [35] A. Tenart, G. Hercé, J.-P. Bureik, A. Dareaux, and D. Clément, Observation of pairs of atoms at opposite momenta in an equilibrium interacting Bose gas, *Nat. Phys.* **17**, 1364 (2021).
- [36] J.-P. Bureik, G. Hercé, M. Allemand, A. Tenart, T. Roscilde, and D. Clément, Suppression of Bogoliubov momentum pairing and emergence of non-Gaussian correlations in ultracold interacting Bose gases, *Nat. Phys.* **21**, 57 (2025).
- [37] S. Brandstetter, C. Heintze, K. Subramanian, P. Hill, P. M. Preiss, M. Galka, and S. Jochim, Magnifying the Wave Function of Interacting Fermionic Atoms, [arXiv:2409.18954](https://arxiv.org/abs/2409.18954) (2024).
- [38] T. de Jongh, J. Verstraten, M. Dixmieras, C. Daix, B. Peaudecerf, and T. Yefsah, Quantum Gas Microscopy of Fermions in the Continuum, [arXiv:2411.08776](https://arxiv.org/abs/2411.08776) (2024).
- [39] J. Xiang, E. Cruz-Colón, C. C. Chua, W. R. Milner, J. de Hond, J. F. Fricke, and W. Ketterle, In situ imaging of the thermal de Broglie wavelength in an ultracold Bose gas, [arXiv:2411.08779](https://arxiv.org/abs/2411.08779) (2024).
- [40] R. Yao, S. Chi, M. Wang, R. J. Fletcher, and M. Zwierlein, Measuring pair correlations in Bose and Fermi gases via atom-resolved microscopy, [arXiv:2411.08780](https://arxiv.org/abs/2411.08780) (2024).
- [41] P. Makotyn, C. E. Klauss, D. L. Goldberger, E. A. Cornell, and D. S. Jin, Universal dynamics of a degenerate unitary Bose gas, *Nat. Phys.* **10**, 116 (2014).
- [42] C. Eigen, J. A. P. Glidden, R. Lopes, E. A. Cornell, R. P. Smith, and Z. Hadzibabic, Universal prethermal dynamics of Bose gases quenched to unitarity, *Nature* **563**, 221 (2018).
- [43] E. A. L. Henn, J. A. Seman, G. Roati, K. M. F. Magalhães, and V. S. Bagnato, Emergence of Turbulence in an Oscillating Bose–Einstein Condensate, *Phys. Rev. Lett.* **103**, 045301 (2009).
- [44] N. Navon, A. L. Gaunt, R. P. Smith, and Z. Hadzibabic, Emergence of a turbulent cascade in a quantum gas, *Nature* **539**, 72 (2016).
- [45] G. K. Batchelor, A. A. Townsend, and H. Jeffreys, The nature of turbulent motion at large wave-numbers, *Proc. R. Soc. Lond. A* **119**, 238 (1949).
- [46] A. C. Newell, S. Nazarenko, and L. Biven, Wave turbulence and intermittency, *Phys. D: Nonlinear Phenom.* **152-153**, 520 (2001).
- [47] O. Firstenberg, T. Peyronel, Q.-Y. Liang, A. V. Gorshkov, M. D. Lukin, and V. Vuletić, Attractive photons in a quantum nonlinear medium, *Nature* **502**, 71 (2013).
- [48] T. F. Schmidutz, I. Gotlibovych, A. L. Gaunt, R. P. Smith, N. Navon, and Z. Hadzibabic, Quantum Joule–Thomson Effect in a Saturated Homogeneous Bose Gas, *Phys. Rev. Lett.* **112**, 040403 (2014).
- [49] J. R. Taylor, *Scattering Theory: The Quantum Theory of Nonrelativistic Collisions* (Dover Publications, Mineola, NY, 2006).
- [50] M. Kardar, *Statistical Physics of Fields* (Cambridge University Press, Cambridge, 2007).

METHODS

Linear response

In Extended Data Fig. 1 we show the recorded photon count versus the time-integrated pulse intensity, verifying that we work in the linear-response regime.

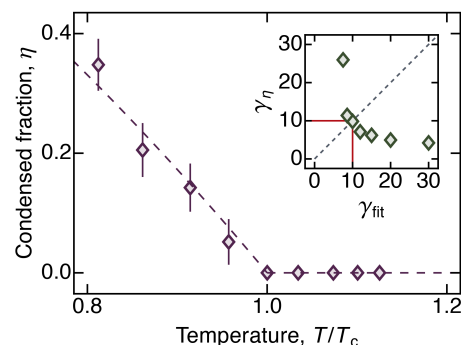


Extended Data Fig. 1. **Linearity of the response.** We show the linearity of the recorded photon count with the time-integrated intensity of the atom-light scattering pulse. We always work with light pulses such that the scattered-photon count is $\lesssim 100$. We estimate that this corresponds to $\lesssim 0.1$ photon scattered per atom.

Optical box trap

Our optical box trap is formed by intersecting two hollow-tube 755 nm laser beams with diameters of $\approx 35 \mu\text{m}$ and $\approx 100 \mu\text{m}$, resulting in a trap volume $V \approx 80 \times 10^3 \mu\text{m}^3$. To extract the thermodynamic properties of our gas, we take absorption images after 20 ms of time-of-flight expansion at weak interactions ($a < 40 a_0$).

To calibrate the steepness of our trap walls we follow



Extended Data Fig. 2. **Box sharpness.** Main panel: temperature dependence of the condensed fraction, obtained using Eq. (S1) with $\gamma_{\text{fit}} = 10$, is fitted well to Eq. (S2) with the consistent $\gamma_\eta = 10$ (dashed line). Inset: γ_η obtained for different γ_{fit} ; the consistency requirement $\gamma_\eta = \gamma_{\text{fit}}$ (dashed line) gives $\gamma = \gamma_\eta = \gamma_{\text{fit}} = 10$.

Ref. [48], assuming an isotropic power-law trapping potential, $U(r) \propto r^\gamma$, for which (assuming an ideal Bose gas) the momentum distribution of the thermal component is

$$f(k) \propto g_{3/\gamma} \left(z \exp \left[-\frac{\hbar^2 k^2}{2mk_B T} \right] \right), \quad (\text{S1})$$

and the condensed fraction for $T < T_c$ is

$$\eta = 1 - \left(\frac{T}{T_c} \right)^{\frac{3}{2} + \frac{3}{\gamma}}, \quad (\text{S2})$$

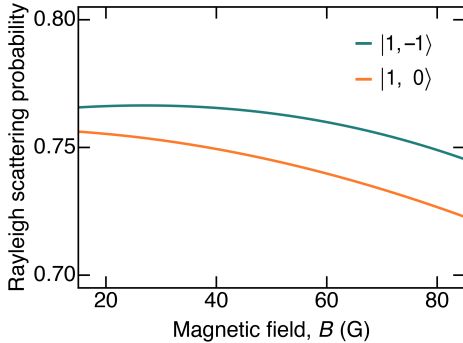
where $g_\alpha(k) = \sum_{x=1}^{\infty} (k^x/x^\alpha)$ is the polylogarithm function, $z = \exp[\mu/(k_B T)]$ the fugacity, and μ the chemical potential. We fit $f(k)$ using different values of γ , denoted γ_{fit} , and then from the deduced $\eta(T/T_c)$ extract another value of γ , denoted γ_η . Self-consistency then requires $\gamma_\eta = \gamma_{\text{fit}}$. As we show in Extended Data Fig. 2, our data is described well by $\gamma = 10$.

Light scattering and collection

We count the scattered photons using an electron multiplying charge-coupled device (EMCCD) camera (PROHS-1024BX3), with a quantum efficiency of 95%, in an imaging system with a numerical aperture of ≈ 0.1 . Hardware binning over 32×32 pixels and a gain of ≈ 100 are used to ensure that photon shot noise dominates over the readout noise. We typically achieve a signal-to-noise ratio of 6.

For each set of E measurements we normalize Γ by the single-particle scattering rate Γ_0 , which we obtain by probing clouds that were allowed to expand in time-of-flight for 10 ms.

In our experiments, with the incoming beam detuned 1 GHz from the 766.7 nm line and having σ^- polarization with respect to its horizontal propagation axis (Fig. 1a), the B field oriented along the vertical axis, and the scattered photons collected at an angle of 35° in the horizontal plane, both spin-preserving (Rayleigh) and spin-changing (Raman) scattering

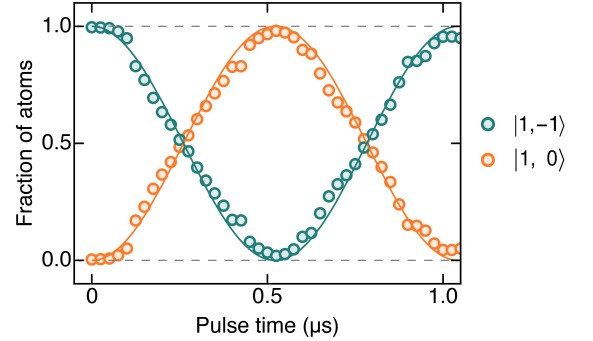


Extended Data Fig. 3. **Probability of Rayleigh scattering.** For our experimental parameters, both our spin states, and all B fields used, calculations give that for single-particle scattering ($\lambda \ll d$) the fraction of scattering events that are spin-preserving is always close to 0.75.

occur, and only the former is bosonically enhanced [5]. In Extended Data Fig. 3, we show for both our spin states the calculated fraction of scattering events that are spin-preserving in the limit of single-particle scattering.

Spin flips

We use a pair of co-propagating laser beams (detuned by 2 GHz from the 766.7 nm line) to implement two-photon Raman transitions between the $|1, -1\rangle$ and $|1, 0\rangle$ spin states at different B fields. In Extended Data Fig. 4, we plot the measured fraction of atoms in each state for a varying Raman-pulse duration, showing a spin-flip (π -pulse) time of $\approx 0.5 \mu\text{s}$.



Extended Data Fig. 4. **Spin transfer.** Fraction of atoms in $|1, -1\rangle$ and $|1, 0\rangle$ states as a function of the Raman-pulse duration. The solid lines show sinusoidal fits that give a Rabi frequency $\Omega/(2\pi) \approx 1$ MHz.

BMF correlations

Here, we focus on the non-trivial part of the structure factor, $\tilde{S}(\mathbf{Q}) = S(\mathbf{Q}) - 1$:

$$\tilde{S}(\mathbf{Q}) = \frac{1}{N} \iint e^{i\mathbf{Q} \cdot (\mathbf{r}_1 - \mathbf{r}_2)} \times \text{Tr} \left[\rho \hat{\psi}^\dagger(\mathbf{r}_1) \hat{\psi}^\dagger(\mathbf{r}_2) \hat{\psi}(\mathbf{r}_2) \hat{\psi}(\mathbf{r}_1) \right] d^3\mathbf{r}_1 d^3\mathbf{r}_2. \quad (\text{S3})$$

At the two-body level, s -wave interaction with scattering length a modifies the non-interacting two-body eigenstates

$$|\mathbf{k}_1, \mathbf{k}_2\rangle_0 = e^{i\mathbf{k}_1 \cdot \mathbf{r}_1} e^{i\mathbf{k}_2 \cdot \mathbf{r}_2}, \quad (\text{S4})$$

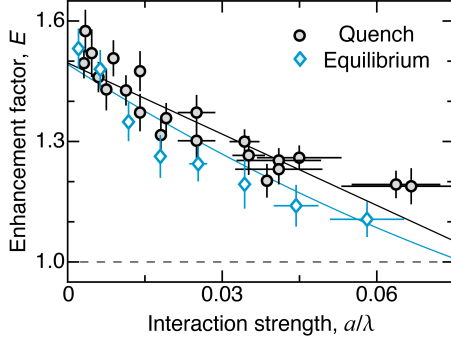
with single-particle momenta $\hbar\mathbf{k}_1$ and $\hbar\mathbf{k}_2$, to

$$|\mathbf{k}_1, \mathbf{k}_2\rangle = e^{i\mathbf{K} \cdot \mathbf{R}} \left[e^{i\mathbf{k} \cdot \mathbf{r}} - a \frac{e^{i\mathbf{k}r}}{r} \right], \quad (\text{S5})$$

where $\mathbf{R} = (\mathbf{r}_1 + \mathbf{r}_2)/2$ and $\mathbf{K} = \mathbf{k}_1 + \mathbf{k}_2$ are the center of mass variables, and $\mathbf{r} = \mathbf{r}_1 - \mathbf{r}_2$ and $\mathbf{k} = (\mathbf{k}_1 - \mathbf{k}_2)/2$ are the relative variables.

The interacting and non-interacting states are related by the Moller operator Ω_+ [49]:

$$|\mathbf{k}_1, \mathbf{k}_2\rangle = \Omega_+ |\mathbf{k}_1, \mathbf{k}_2\rangle_0. \quad (\text{S6})$$



Extended Data Fig. 5. **Additional equilibrium measurements.** For $n = 10 \mu\text{m}^{-3}$ and $T = T_c$, we plot equilibrium $E(a/\lambda)$ (blue), obtained as in Fig. 2, alongside the post-quench data from Fig. 3c (black). The equilibrium data includes both MF and BMF suppression of E for a specific a/λ , whereas in the post-quench data the MF contribution is small and independent of a , because the density distribution remains that of the (pre-quench) quasi-ideal gas. The solid lines show our calculations for the two experimental scenarios.

For bosons, in terms of field operators:

$$\begin{aligned} \Omega_+ = \mathbb{I} + \frac{i}{2} \iiint \alpha(\mathbf{k}_1, \mathbf{k}_2 \rightarrow \mathbf{k}'_1, \mathbf{k}'_2) \\ \times \hat{\psi}^\dagger(\mathbf{k}'_1) \hat{\psi}^\dagger(\mathbf{k}'_2) \hat{\psi}(\mathbf{k}_2) \hat{\psi}(\mathbf{k}_1) \quad (\text{S7}) \\ \times \frac{d^3\mathbf{k}_1}{(2\pi)^3} \frac{d^3\mathbf{k}_2}{(2\pi)^3} \frac{d^3\mathbf{k}'_1}{(2\pi)^3} \frac{d^3\mathbf{k}'_2}{(2\pi)^3}, \end{aligned}$$

where \mathbb{I} is the identity operator and

$$\begin{aligned} \alpha(\mathbf{k}_1, \mathbf{k}_2 \rightarrow \mathbf{k}'_1, \mathbf{k}'_2) = (2\pi)^3 \delta(\mathbf{k}'_1 + \mathbf{k}'_2 - \mathbf{k}_1 - \mathbf{k}_2) \\ \times 4\pi i \frac{a}{k'^2 - k^2 - i\epsilon}, \quad (\text{S8}) \end{aligned}$$

where $k' = |\mathbf{k}'_1 - \mathbf{k}'_2|/2$ and $k = |\mathbf{k}_1 - \mathbf{k}_2|/2$.

For a dilute gas, we consider only pairwise corrections to the many-body wave function, which is the leading-order approximation. This amounts to expressing the thermal density matrix ρ as [28]

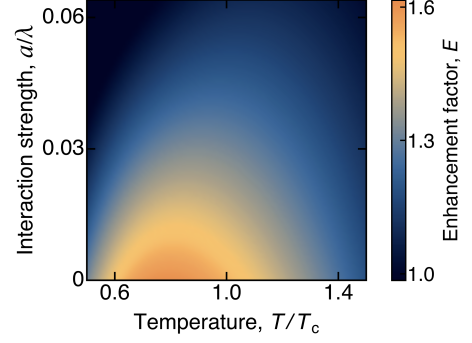
$$\rho \simeq \Omega_+ \rho_0 \Omega_+^\dagger, \quad (\text{S9})$$

where ρ_0 is the non-interacting thermal density matrix.

Using Eqs. (S7)-(S9) and denoting $\tilde{S}_0(\mathbf{Q})$ the $a = 0$ value of $\tilde{S}(\mathbf{Q})$, we obtain:

$$\begin{aligned} \tilde{S}(\mathbf{Q}) = \\ \tilde{S}_0(\mathbf{Q}) - \frac{16\pi a}{nQ^2} \iint \frac{N_{\mathbf{k}_1} N_{\mathbf{k}_2}}{1 + \mathbf{Q} \cdot (\mathbf{k}_1 - \mathbf{k}_2)/Q^2} \frac{d^3\mathbf{k}_1}{(2\pi)^3} \frac{d^3\mathbf{k}_2}{(2\pi)^3}, \quad (\text{S10}) \end{aligned}$$

where $N_{\mathbf{k}} = 1/(z^{-1} \exp[\hbar^2 k^2 / (2mk_B T)] - 1)$. Note that this approach is formally equivalent to first-order perturbation theory using the contact interaction potential, and that for high



Extended Data Fig. 6. **Additional equilibrium calculations.** We plot the calculated E versus T/T_c and a/λ for $n = 10 \mu\text{m}^{-3}$, including both MF (density) and BMF (correlations) effects.

temperature ($\lambda/d \ll 1$) and low recoil momentum ($Q\lambda \ll 1$) Eq. (S10) reduces to the result previously obtained in [5]:

$$\tilde{S}(\mathbf{Q}) = \tilde{S}_0(\mathbf{Q}) \left(1 - 8\sqrt{2} a/\lambda\right). \quad (\text{S11})$$

To compare these calculations to our measurements of E , we: (i) account for our beam polarisation, and (ii) use the mean-field (MF) density distribution within the local-density approximation to calculate the local scattering rate, and then integrate it over the trap.

Specifically, for Fig. 3c we calculate the MF distribution for the initial small a (in state $|1, -1\rangle$) and the BMF effects for the final a (in state $|1, 0\rangle$), because on the timescale of the measurements the density distribution does not adjust to the change in a . As a complement to those measurements, in Extended Data Fig. 5 we also show additional measurements taken in equilibrium (as in Fig. 2), for the same $n = 10 \mu\text{m}^{-3}$ and $T = T_c$. In the latter case the different a values correspond to both different density distributions (MF effect) and different correlations (BMF effect), and the total reduction of E with a/λ is similar but slightly larger.

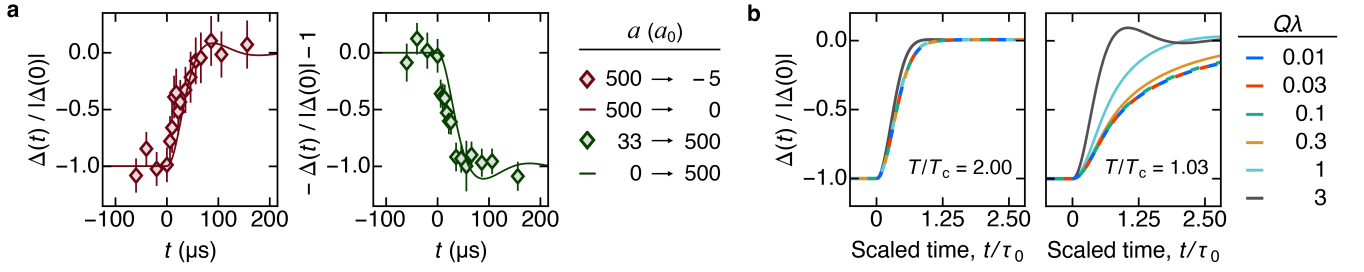
Finally, in Extended Data Fig. 6 we show our equilibrium calculations (including both MF and BMF effects) for a range of a/λ and T/T_c values, for our setup and $n = 10 \mu\text{m}^{-3}$.

Quench dynamics

In Extended Data Fig. 7 we compare our data from Fig. 3b to numerical calculations of the evolution of the structure factor after an interaction quench, and also show additional simulations for different $Q\lambda$ and T/T_c . In these calculations we assume a homogeneous cloud and quenches $a \rightarrow 0$ or vice versa.

For the $a \rightarrow 0$ case, starting with the interacting thermal density matrix [Eq. (S9)], the dynamics are simply given by the evolution under the non-interacting Hamiltonian H_0 :

$$\rho(t) = e^{-iH_0 t/\hbar} \left(\Omega_+ \rho_0 \Omega_+^\dagger \right) e^{iH_0 t/\hbar}. \quad (\text{S12})$$



Extended Data Fig. 7. **Quench dynamics.** **a**, Our calculations (solid lines) of $\Delta(t)/|\Delta(0)|$ capture the data from Fig. 3b (diamonds). Note that the calculations and the data are each normalized with their respective $|\Delta(0)|$. **b**, Well above T_c (left), the correlation length ξ is of order λ and $\Delta(t)/|\Delta(0)|$ is for $Q \lesssim 1/\lambda$ a universal function of t/τ_0 , where $\tau_0 = m\lambda/(\hbar Q)$. Close to T_c (right), ξ grows, the dynamics are universal only for $Q \lesssim 1/\xi$ (here $Q \lesssim 0.1/\lambda$), and these universal dynamics are slower.

Dropping the Q labels and writing

$$\tilde{S}(t) = \Delta(t) + \tilde{S}_0, \quad (\text{S13})$$

such that $\Delta(0) = \tilde{S} - \tilde{S}_0$ (which is negative for $a > 0$) and $\Delta(\infty) = 0$, we get:

$$\begin{aligned} \Delta(t) = & -\frac{16\pi a}{nQ^2} \iint \frac{N_{\mathbf{k}_1} N_{\mathbf{k}_2}}{1 + \mathbf{Q} \cdot (\mathbf{k}_1 - \mathbf{k}_2)/Q^2} \\ & \times \cos\left(\frac{\hbar Q^2 [1 + \mathbf{Q} \cdot (\mathbf{k}_1 - \mathbf{k}_2)/Q^2] t}{m}\right) \frac{d^3 \mathbf{k}_1}{(2\pi)^3} \frac{d^3 \mathbf{k}_2}{(2\pi)^3}. \end{aligned} \quad (\text{S14})$$

For the $0 \rightarrow a$ case, we start with ρ_0 and propagate it with the interacting Hamiltonian. Treating the interactions using first-order perturbation theory gives

$$\tilde{S}(t) = \tilde{S} - \Delta(t), \quad (\text{S15})$$

again with the $\Delta(t)$ given in Eq. (S14), *i.e.*, at this level of approximation the dynamics are completely symmetric.

It is instructive to rewrite Eq. (S14) as

$$\Delta(t) = -\frac{16\pi \hbar a n}{m} \int_t^\infty \sin\left(\frac{\hbar Q^2 t'}{m}\right) \left|g^{(1)}\left(\frac{\hbar Q t'}{m}\right)\right|^2 dt', \quad (\text{S16})$$

where

$$g^{(1)}(r) = \frac{1}{N} \int \text{Tr} \left[\rho \hat{\psi}^\dagger(\mathbf{r}' + \mathbf{r}) \hat{\psi}(\mathbf{r}') \right] d^3 \mathbf{r}' \quad (\text{S17})$$

is the normalized first-order correlation function, which decays over the correlation length ξ . This shows that the temporal decay of $\Delta(t)$ is directly related to the spatial decay of $g^{(1)}(r)$, with the characteristic relaxation time set by $m\xi/(\hbar Q)$. Well above T_c , where $g^{(1)}(r) = \exp(-\pi r^2/\lambda^2)$, so ξ is of order λ , the characteristic relaxation time $\tau_0 = m\lambda/(\hbar Q)$ can be interpreted as the time it takes for particles with typical thermal velocity $\hbar/(m\lambda)$ to travel across the lengthscale $1/Q$, over which the correlations are probed by the light scattering. However, as $T \rightarrow T_c$, the relaxation dynamics slow down due to the growth of ξ [50].

Also note that for $Q \ll 1/\xi$, the sine function in Eq. (S16) can be linearized, and the relaxation dynamics for different Q follow a universal trajectory

$$\Delta(t) = -16\pi n \lambda^3 \frac{a}{\lambda} \int_t^\infty \frac{t'}{\tau_0} \left|g^{(1)}\left(\lambda \frac{t'}{\tau_0}\right)\right|^2 \frac{dt'}{\tau_0}. \quad (\text{S18})$$

For $T/T_c \gg 1$, this gives $\Delta(t) = \Delta(0) \exp(-2\pi(t/\tau_0)^2)$, with the universal regime extending to $Q \simeq 1/\lambda$. Approaching T_c , the universal function develops a heavier tail and the extent of the universal regime shrinks (see Extended Data Fig. 7b). For $Q \gtrsim 1/\xi$, the dynamics are more intricate, with $\Delta(t)$ exhibiting damped coherent oscillations. Such oscillatory behavior is predicted for our measurements at T_c , but experimentally we do not resolve these small oscillations within our errors.